Volume 5 | Number 24 | 21 December 2014 | Pages 6869–7136

Polymer Chemistry

www.rsc.org/polymers

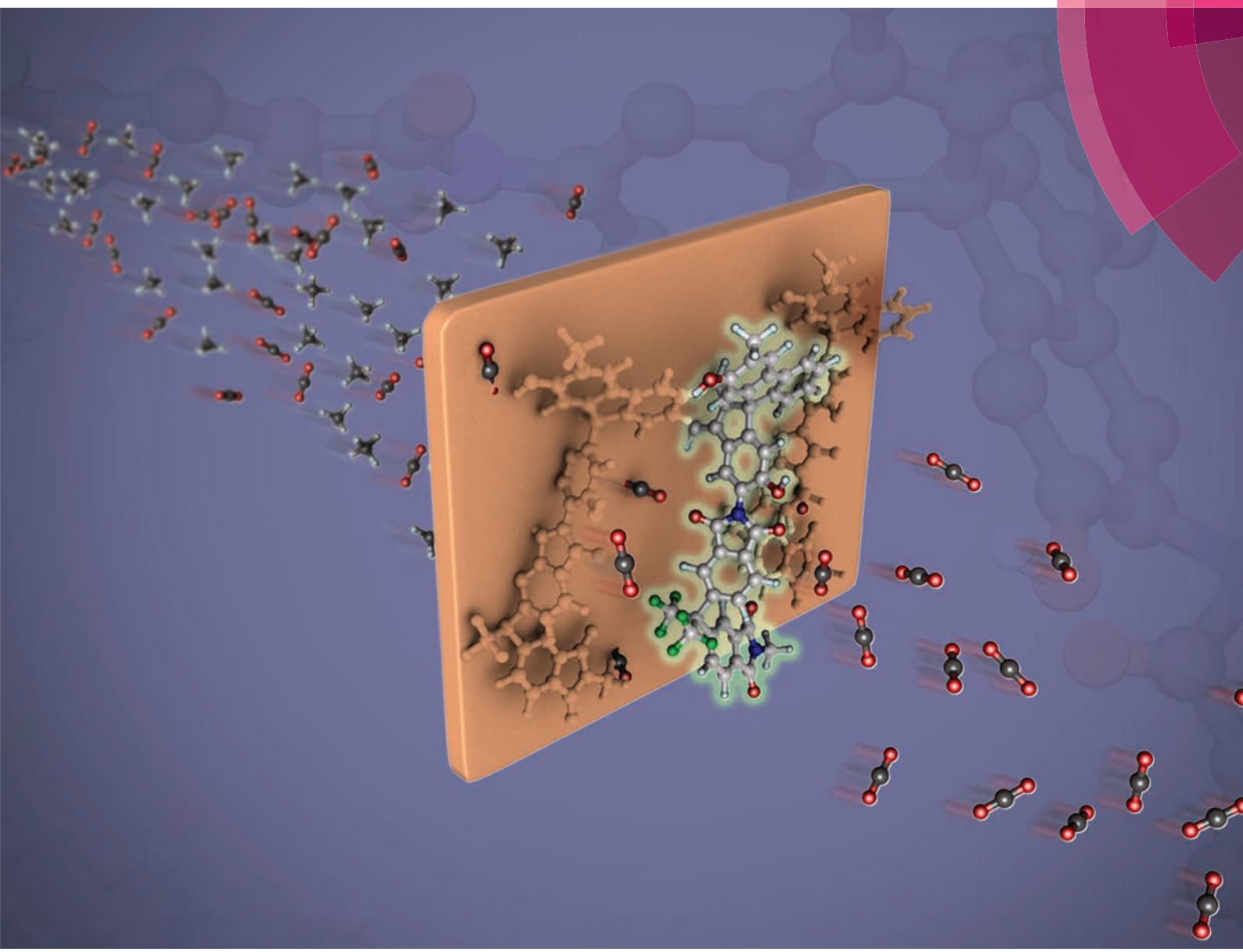

ISSN 1759-9954

ROYAL SOCIETY OF CHEMISTRY

PAPER
Ingo Pinnau *et al.*
Pristine and thermally-rearranged gas separation membranes from novel *o*-hydroxyl-functionalized spirobifluorene-based polyimides

Polymer Chemistry

PAPER

View Article Online
View Journal | View Issue

Cite this: *Polym. Chem.*, 2014, **5**, 6914

Pristine and thermally-rearranged gas separation membranes from novel *o*-hydroxyl-functionalized spirobifluorene-based polyimides†

Xiaohua Ma, Octavio Salinas, Eric Litwiller and Ingo Pinnau*

Received 3rd September 2014,
Accepted 20th September 2014

DOI: 10.1039/c4py01221f

www.rsc.org/polymers

A novel *o*-hydroxyl-functionalized spirobifluorene-based diamine monomer, 2,2′-dihydroxyl-9,9′-spirobifluorene-3,3′-diamine (HSBF), was successfully prepared by a universal synthetic method. Two *o*-hydroxyl-containing polyimides, denoted as 6FDA-HSBF and SPDA-HSBF, were synthesized and characterized. The BET surface areas of 6FDA-HSBF and SPDA-HSBF are 70 and 464 $m^2\ g^{-1}$, respectively. To date, SPDA-HSBF exhibits the highest CO_2 permeability (568 Barrer) among all hydroxyl-containing polyimides. The HSBF-based polyimides exhibited higher CO_2/CH_4 selectivity than their spirobifluorene (SBF) analogues (42 for 6FDA-HSBF *vs.* 27 for 6FDA-SBF) due to an increase in their diffusivity selectivity. Polybenzoxazole (PBO) membranes obtained from HSBF-based polyimide precursors by thermal rearrangement showed enhanced permeability but at the cost of significantly decreased selectivity.

Introduction

Membrane-based gas separation is a well-established industrial technology with great potential for a wide variety of large-scale industrial applications, such as natural gas sweetening, hydrogen recovery, on-site nitrogen generation, and CO_2 separation from flue gas.[1–3] An ideal membrane is characterized by both high permeability and selectivity. Generally, there is a trade-off in the performance of polymeric membranes, often referred to as the Robeson upper bound,[4,5] in which materials with higher permeability exhibit lower selectivity and *vice versa*. However, rational molecular design can provide an efficient way to create novel polymeric membranes with superior gas transport properties. One strategy is to introduce micropores (<20 Å) or ultra-micropores (<7 Å) into polymers to form intrinsically microporous polymers (PIMs). The prototype glassy PIM, linear chain poly(1-trimethyl-silyl-1-propyne) (PTMSP), first reported in 1983, is still one of the highest permeable materials to date due to inefficient chain packing resulting from its highly rigid main chain and a bulky trimethylsilyl side group.[6,7] PTMSP and other di-substituted polyacetylenes exhibit exceptionally high gas and organic vapor permeability. Furthermore, PTMSP shows the highest mixed C_{3+} hydrocarbon/CH_4 and C_{3+} hydrocarbon/H_2 selectivity of all known polymers.[7–9] In 2004, a new class of spirobisindane-based ladder PIMs was reported by Mckeown and Budd.[10–12] These rigid glassy polymers consist of contorted spiro-centers linked with fused dioxane rings that prevent efficient polymer chain packing. Many ladder-type PIMs are solution processable from a variety of solvents (*e.g.* chloroform, THF, *etc.*) and, therefore, can be readily processed into membranes. Ladder PIMs show promising gas and vapor separation performance,[13–16] and extensive investigations have been applied to PIM-1 and its analogues, including a spirobifluorene (SBF) ladder PIM.[17–31] Recently, significant advances have been achieved with the development of AB-type triptycene- (TPIM-1 and TPIM-2)[32] and Tröger-based[33] ladder polymers that significantly outperform all polymers listed on the 2008 Robeson upper bound for O_2/N_2, H_2/N_2 and H_2/CH_4 separation.

The concept of introducing intrinsic micropores into glassy polymers has also been extended to polyimides (PI). Ghanem *et al.*[34,35] and Rogan *et al.*[36] reported spirobisindane dianhydride-based PIM-PIs, which exhibit significantly improved permeability among all known polyimides. For example, PIM-PI-8 showed a CO_2 permeability of 3700 Barrer combined with a moderate pure-gas CO_2/CH_4 selectivity of 13.[35] PIM-PIs based on triptycene diamines have shown higher selectivity but at the cost of lower permeability; *e.g.* 6FDA-2,6-diaminotriptycene (DATRI) showed a CO_2 permeability of 189 Barrer and a CO_2/CH_4 selectivity of 30.5.[37,38] Recently, Ghanem *et al.* and Swaidan *et al.*[39,40] reported a series of PIM-PIs made from 9,10-bridgehead-substituted triptycene dianhydrides, which

Advanced Membranes and Porous Materials Center, Physical Sciences and Engineering Division, King Abdullah University of Science and Technology, Thuwal 23955-6900, Saudi Arabia. E-mail: ingo.pinnau@kaust.edu.sa; Fax: +966 02 80821328

†Electronic supplementary information (ESI) available: Solubility, FT-IR, and wide-angle X-ray scattering of the polymers before and after TR. See DOI: 10.1039/c4py01221f

significantly surpassed the 2008 upper bound for several gas pairs due to their strong size-sieving ultramicroporous structures. A rigid ethanoanthracene dianhydride-based polyimide (PIM-EA-TB) reported by Rogan *et al.* also gave excellent gas permeation results.[41]

Another efficient way to generate micropores is to form polybenzoxazoles (PBO) from *o*-hydroxyl-containing polyimide precursors by thermal rearrangement (TR), typically in the range of 400 to 450 °C.[42–44] The resulting PBOs exhibit significant increase in gas permeability as well as enhanced chemical and thermal stability. For example, the PBO of 6FDA-bisAPAF polyimide shows a CO_2 permeability of 1600 Barrer, and a CO_2/CH_4 selectivity of 45, which lies well above the 2008 Robeson upper bound. The TR method has also successfully been applied to a variety of other polymer precursors, such as polyetherimides,[45] polypyrrolones,[46] *etc.* However, the development of a larger variety of TR-generated PBOs has been restricted due to the availability of only a few commercially available *o*-hydroxyl diamines, such as 3,3-dihydroxy-4,4-diaminobiphenyl (HAB),[47] 2,2-bis(3-amino-4-hydroxy-phenyl) hexafluoropropane (APAF), 4,6-diamino resorcinol,[48] and 2,4-diaminophenol.[49]

Recently, a newly developed *o*-hydroxyl functionalized spirobisindane-based diamine was introduced by Ma *et al.*[50] and Li *et al.*[51] and used for the first TR-based PBOs from PIM-PIs (Scheme 1). A several-fold increase of gas permeability was observed with a drop in selectivity. Similar results were also observed by Shamsipur *et al.* using T-PIM-PI-OH-1 as the PBO precursor.[49] The effect of precursor microporosity on TR PBO performance still needs further investigation.

In this study, a general method for synthesis of *o*-hydroxyl-functionalized aromatic diamine monomers is reported. For example, the synthesis of a novel monomer, 2,2′-dihydroxyl-9,9′-spirobifluorene-2,2′-diamine (HSBF), is shown in Scheme 2. Two *ortho*-hydroxyl containing polyimides were made by one-pot polycondensation reaction with two dianhydrides, 6FDA and SPDA, respectively. Furthermore, the polyimides were heat-treated to produce PBO membranes by thermal re-arrangement.

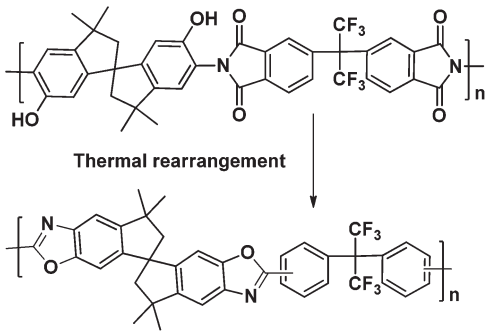

Scheme 1 Structure of PIM-6FDA-OH and its corresponding polybenzoxazole (6FDA-SP-PBO).

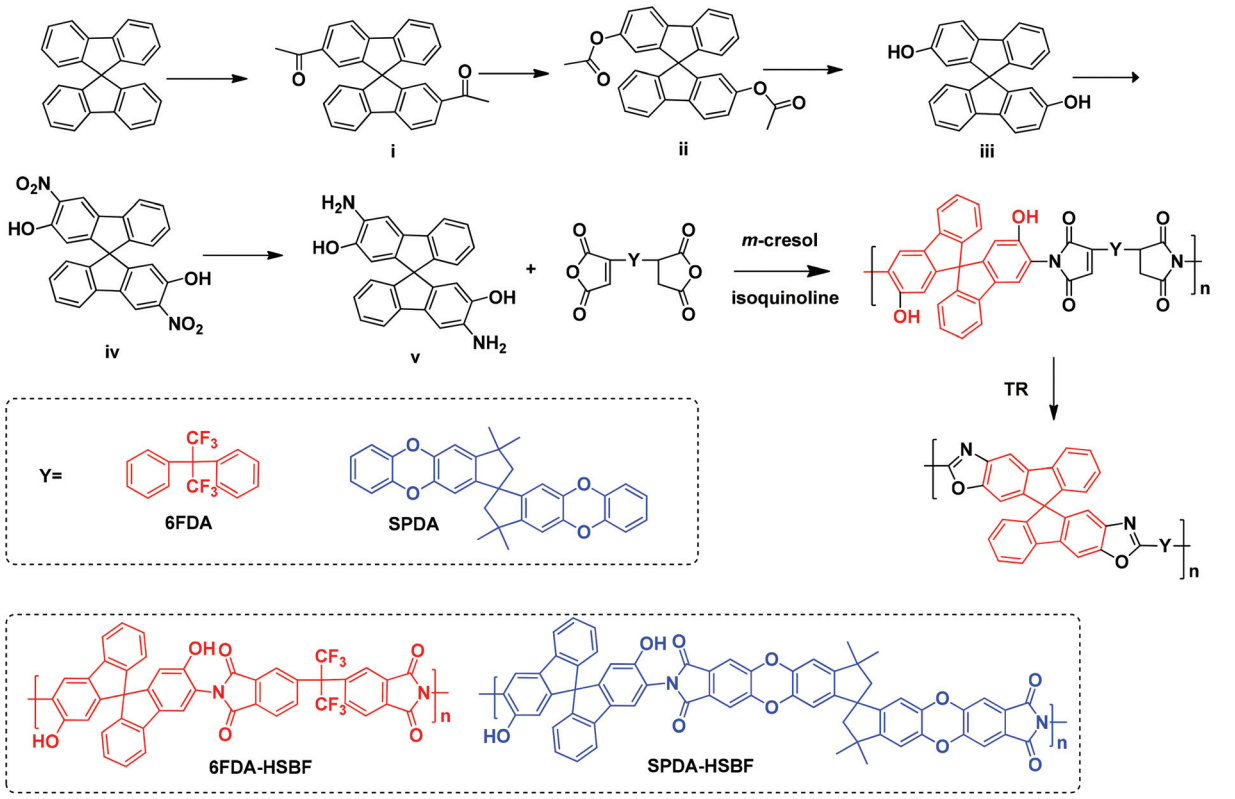

Scheme 2 Synthetic route of the HSBF monomer (v), HSBF-based polyimides, and their thermally-rearranged polybenzoxazoles.

Experimental

Materials

4,4′-(Hexafluoroisopropylidene)diphthalic anhydride (6FDA, 99%) was obtained from Sigma-Aldrich and purified by sublimation before use. 9,9-Spirobifluorene, *m*-cresol, acetic chloride, aluminum trichloride, palladium on carbon (10%), dichloromethane, tetrahydrofuran, petrol oil ether, *m*-chloroperoxybenzoic acid (*m*-cpba), potassium carbonate, sodium hydroxide, ethyl acetate, acetic acid, nitric acid and *N*,*N*′-dimethylformamide were obtained from Sigma-Aldrich and used as received. Spirobisindane-based dianhydride (SPDA) was synthesized according to a previously reported method and dried at 120 °C under vacuum overnight prior to use.[35] Polyimides without OH group, 6FDA-SBF and SPDA-SBF, were prepared as described in our previous report.[52]

Characterization and methods

^{1}H NMR and ^{13}C NMR spectra of the newly synthesized monomer and polymers were recorded with a Bruker AVANCE-III spectrometer at a frequency of 400 MHz in either deuterated chloroform or deuterated dimethylsulfone with tetramethylsilane as an internal standard and recorded in ppm. Elemental analysis was carried out using a Perkin-Elmer 2400 elemental analyzer. High-resolution mass spectroscopy (HRMS) was conducted on a Thermo LC/MS system with LTQ Orbitrap Velos detectors. Fourier transform infrared spectra (FT-IR) of the polyimides and their TR-based PBOs were acquired using a Varian 670-IR FT-IR spectrometer. Molecular weights (M_n) and molecular weight distribution (PDI) of the polymers were obtained by gel permeation chromatography (Agilent GPC 1200) with polystyrene as an external standard. X-ray scattering was conducted on a Bruker D8 Advance diffractometer with a scanning rate of 0.5° min^{-1} from 6 to 50°. Thermal gravimetric analysis (TGA) of the polymers was carried out using a TGA Q5000 under a N_2 atmosphere from room temperature to 800 °C at a heating rate of 3 °C min^{-1}. The BET surface areas of the polymers and their thermally-rearranged membranes were measured by N_2 sorption at 77 K (Micrometrics ASAP 2020); each of the samples was degassed at 150 °C for 12 h before testing.

Synthesis

2,2′-Diacetyl-9,9′-spirobifluorene (i). Aluminum trichloride (12.6 g, 94.5 mmol) and acetic chloride (6.20 g, 79.0 mmol) were dissolved in 200 mL dichloromethane and cooled to 0 °C using an ice-bath. 9,9′-Spirobifluorene (10.0 g, 31.6 mmol) was dissolved in 60 mL dichloromethane and then added dropwise over 2 h. Thereafter, the reaction system was stirred overnight and poured into ice water (300 mL). The organic phase was separated by a separatory funnel and washed twice with saturated K_2CO_3 (aq.) and water. The organic phase was removed and the residue was purified by column chromatography. The final product was obtained as an off-white solid (9.0 g, yield: 71%). ^{1}H NMR ($CDCl_3$, 400 MHz): δ 8.09 (d, 2H, J = 8.04 Hz), 7.95–7.99 (m, 4H), 7.45 (t, 2H, J = 7.44 Hz, 7.44 Hz), 7.34 (s, 2H), 7.21 (t, 2H, J = 7.48 Hz, 7.48 Hz), 6.76 (d, 2H, J = 7.6 Hz), 2.52 (s, 6H).

2,2′-Diacetoxy-9,9′-spirobifluorene (ii). 2,2′-Diacetyl-9,9′-spirobifluorene (4.08 g, 10.0 mmol) and *m*-cpba (70%, 6.71 g, 27.3 mmol) were dissolved in 240 mL dichloromethane and stirred at room temperature for 10 h. Thereafter, the solution was refluxed for 10 h, and then washed with saturated K_2CO_3 (aq.) and water, respectively. The organic phase was dried with magnesium sulfate. The solvent was removed by rota-evaporation and the residue was purified by column chromatography; the final product was obtained as an off-white solid (3.50 g, yield: 81%). TLC: dichloromethane, R_f = 0.75; ^{1}H NMR (400 MHz, $CDCl_3$): δ 7.85 (t, 4H, J = 8.44 Hz), 7.41 (t, 2H, J = 7.44 Hz), 7.14–7.20 (m, 4H), 6.80 (d, 2H, J = 7.6 Hz), 6.52 (d, 2H, J = 2.04 Hz), 2.21 (s, 6H).

2,2′-Dihydroxyl-9,9′-spirobifluorene (iii). 2,2′-Diacetoxy-9,9′-spirobifluorene (8.40 g, 19.4 mmol) was dissolved in 300 mL methanol. Aqueous NaOH solution (1.68 g, 42.0 mmol) dissolved in water (56 mL) was added dropwise, and the solution was continuously stirred under N_2 overnight at room temperature. HCl (2 N, 30 mL) was added to neutralize the reaction. Most of the methanol was removed by rota-evaporation, and an off-white solid product was obtained by precipitation in water (300 mL). The vacuum-dried white powder (6.00 g, yield: 88.7%) was obtained after recrystallization from the ethyl acetate–ligroin mixed solvent. TLC: ethyl acetate–ligroin = 1/1, R_f = 0.5; ^{1}H NMR (400 MHz, $CDCl_3$): δ 7.72–7.79 (m, 4H), 7.38 (t, 2H, J = 8.0 Hz, 8.0 Hz), 7.10 (t, 2H, J = 8.0 Hz, 8.0 Hz), 6.87–6.90 (m, 2H), 6.77 (d, 2H, J = 8.0 Hz), 6.24 (s, 2H).

3,3′-Dinitrol-2,2′-dihydroxyl-9.9′-spirobifluorene (iv). 2,2′-Dihydroxyl-9,9′-spirobifluorene (696 mg, 2.00 mmol) was dissolved in 20 mL acetic acid and HNO_3 (4 N, 1.10 mL) was added dropwise over 30 minutes. The solution was stirred overnight, filtered and washed with ethanol and then water. After drying in an oven at 100 °C overnight, a yellow powder (580 mg, yield: 66.2%) as a mixture of isomers was obtained. The symmetric isomer was obtained by column chromatography as a light yellow solid (320 mg, yield: 36.5%). TLC: dichloromethane–ligroin = 1/1, R_f = 0.35. ^{1}H NMR (400 MHz, $CDCl_3$): δ 10.75 (s, 2H), 8.54 (s, 2H), 7.87 (d, 2H, J = 7.72 Hz), 7.45 (t, 2H, J = 7.56 Hz, 7.56 Hz), 7.20 (t, 2H, J = 7.54 Hz, 7.54 Hz), 6.75 (d, 2H, J = 7.64 Hz), 6.50 (s, 2H). ^{13}C NMR (100 MHz, $CDCl_3$): δ 158.40, 155.72, 146.97, 139.18, 134.43, 133.81, 129.13, 129.01, 124.38, 120.54, 116.12, 115.48, 65.77.

3,3′-Diamino-2,2′-dihydroxyl-9,9′-spirobifluorene (v). 3,3′-Dinitrol-2,2′-dihydroxyl-9.9′-spirobifluorene (1.31 g, 30.0 mmol) was dissolved in THF and DMF (15/15 mL) mixed solvent in a 100 mL autoclave. Then, palladium on carbon (0.5 g, 10%) was added in one portion under a N_2 atmosphere. The reaction system was filled with H_2 up to 1.5 MPa, and stirred at 40 °C for 24 h. After cooling to room temperature, the solution was filtered through celite, and then washed with DMF (10 mL) three times before being precipitated in a hexane–dichloromethane mixture (200 mL/100 mL). The precipitate was filtered and dried. Finally, the pure monomer was obtained by vacuum sublimation. ^{1}H NMR (400 MHz, DMSO-

d_6): δ 9.00 (s, 2H), 7.60 (d, 2H, J = 7.52 Hz), 7.22 (t, 2H, J = 7.44 Hz, 7.44 Hz), 7.09 (s, 2H), 6.92 (t, 2H, J = 7.44 Hz, 7.44 Hz), 6.47 (d, 2H, J = 7.52 Hz), 5.93 (s, 2H),4.60 (s, 4H). ^{13}C NMR (100 MHz, DMSO-d_6): δ 149.9, 145.2, 142.8, 138.0, 137.0, 132.8, 127.7, 126.0, 123.4, 118.8, 109.6, 105.8, 64.9. HRMS (ESI): for $C_{25}H_{19}N_2O_2^+$ $[M + H]^+$, 379.1441, found, 379.1428. Anal. Calcd for $C_{25}H_{18}N_2O_2$: C, 79.35; H, 4.79; N, 7.40. Found: C, 79.14; H, 4.11; N, 8.55.

Synthesis of 6FDA-HSBF polyimide. 3,3′-Diamino-2,2′-dihydroxyl-9,9′-spirobifluorene (**iv**) (378.1 mg, 1.00 mmol) and 6FDA (444.4 mg, 1.00 mmol) were added to *m*-cresol (5.0 mL) under stirring at 60 °C for 1 h to form a clear solution. Isoquinoline (3 drops) was added and the system was heated gradually to 180 °C and kept for 8 h before being poured into methanol. The residual *m*-cresol was removed using Soxhlet extraction. The crude product was dissolved in THF and reprecipitated in methanol. A pale yellow polymer was obtained (750 mg, yield: 95%). ^{1}H NMR (400 MHz, DMSO-d_6): δ 10.0 (s, 2H), 8.25 (d, 2H, J = 7.64 Hz), 8.04 (s, 2H), 8.00 (s, 2H), 7.88 (s, 4H), 7.44 (s, 2H), 7.16 (s, 2H), 6.77 (s, 2H), 6.32 (s, 2H). FT-IR (polymer film, ν, cm^{-1}): 3200–3500 (s, br, –OH), 3025 (s, m, C–H), 2920 (s, m, C–H), 1715 (s, str, imide), 1200–1420 (m, str, ph). Molecular weight: M_n = 2.89 × 10^4 g mol^{-1}, PDI = 2.41. S_{BET} = 70 m^2 g^{-1}.

Synthesis of SPDA-HSBF polyimide. The synthetic procedure for SPDA-HSBF was the same as described for 6FDA-HSBF. The polymer SPDA-HSBF was obtained as yellow filaments with a yield of 94%. ^{1}H NMR (400 MHz, DMSO-d_6): δ 9.94 (s, 2H), 8.54 (s, 2H), 7.74–7.90 (m, 4H), 7.48 (d, 2H, J = 2.72 Hz), 7.36 (d, 2H, J = 3.2 Hz), 6.98–7.09 (m, 4H), 6.54–6.70 (m, 4H), 6.05–6.37 (m, 4H), 2.30 (s, 2H), 2.14 (s, 2H), 1.21–1.37 (m, 12H). FT-IR (polymer film, ν, cm^{-1}): 3200–3500 (s, br, –OH), 3025 (s, m, C–H), 2920 (s, m, C–H), 1715 (s, str, imide), 1200–1420 (m, str, ph). Molecular weight: M_n = 4.24 × 10^4 g mol^{-1}, PDI = 2.30. S_{BET} = 464 m^2 g^{-1}.

PI membrane fabrication

The polymers were dissolved in THF (2–3% wt/v) and then filtered using 1.0 μm PTFE filter cartridges. The solution was carefully transferred into a stainless steel ring supported by a leveled glass plate; thereafter, the solvent was slowly evaporated in an oven at 35 °C. After 2 days, the essentially dry membranes (~80 to 100 μm thick) were soaked in a mixture of *n*-hexane–dichloromethane (80/20) for 24 h, air-dried for 24 h and then dried at 120 °C for 24 h under high vacuum. Finally, the membranes were heated to 250 °C under a N_2 atmosphere in a furnace for 2 h to remove any remaining solvent.

PBO membrane formation

The pristine 6FDA-HSBF and SPDA-HSBF films were heated from room temperature to the target temperature at 3 °C min^{-1} under a N_2 atmosphere. The final heating conditions for the two polyimides were set at: (i) 420 °C and soaked 4 h for 6FDA-HSBF and (ii) 450 °C and soaked 2 h for SPDA-HSBF.

Gas permeation measurements

The gas permeability of the membranes was determined using the constant-volume/variable-pressure method. The membranes were degassed in the permeation system on both sides under high vacuum at 35 °C for at least 24 h. The increase in permeate pressure with time was measured by a MKS Baratron transducer. The permeability of all gases was measured using an upstream pressure of 2 bar at 35 °C and was determined by

$$P = D \times S = 10^{10} \times \frac{V_d \times l}{p_{up} \times T \times R \times A} \times \frac{dp}{dt}$$

where P is the permeability (Barrer) – 1 Barrer = 10^{-10} cm^3(STP) cm cm^{-2} s^{-1} cmHg^{-1}, p_{up} is the upstream pressure (cmHg), dp/dt is the steady-state permeate-side pressure increase (cmHg s^{-1}), V_d is the calibrated permeate volume (cm^3), l is the membrane thickness (cm), A is the effective membrane area (cm^2), T is the operating temperature (K), and R is the gas constant (0.278 cm^3 cmHg cm^{-3}(STP) K^{-1}). The apparent diffusion coefficient D (cm^2 s^{-1}) of the polymer membrane was calculated by $D = l^2/6\theta$, where l is the membrane thickness and θ is the time lag of the permeability measurement. The solubility coefficient S (cm^3(STP) cm^{-3} cmHg^{-1}) was obtained from the relationship $S = P/D$.

Results and discussion

The novel diamine, HSBF, was synthesized from 9,9′-spirobifluorene *via* a five-step procedure. Firstly, the 9,9′-spirobifluorene was converted to 2,2′-diacetyl-9,9′-spirobifluorene (**i**) *via* Friedel–Crafts reaction in the presence of aluminum trichloride as a Lewis acid catalyst. The ketone intermediate (**i**) was then selectively converted to the 2,2′-diacetoxy-9,9′-spirobifluorene (**ii**) *via* Baeyer–Villiger oxidation reaction, as previously reported.[53] By hydrolysis under basic conditions, the 2,2′-dihydroxyl-9,9′-spirobifluorene (**iii**) was obtained. It was then further reacted with dilute nitric acid to give the dinitrol intermediate, similar to the previously reported 6,6′-dihydroxyl-spirobisindane.[50] The presence of electron donating OH groups enhanced the activity of both nearby carbon atoms, giving the dinitrol substitution with both the symmetric and asymmetric counterparts (positions 1 and 3 in the 9,9′-spirobifluorene structure). The symmetric dinitrol intermediate (**iv**) was then reduced to the monomer 3,3′-diamino-2,2′-dihydroxyl-9,9′-spirobifluorene (**v**), which was identified and confirmed by ^{1}H and ^{13}C NMR, HRMS, and elemental analysis.

This synthetic procedure provides a general method for the formation of *o*-hydroxyl functionalized diamines directly from aromatic compounds. Two novel hydroxyl (HSBF) containing polyimides were obtained by cycloimidization condensation reaction with two different dianhydrides (6FDA and SPDA), using a one-step high temperature azeotropic method. Their proton NMR (shown in Fig. 1) clearly indicates the presence of hydroxyl groups with a chemical shift from 9.5 to 10 ppm, similar to previously reported hydroxyl-based polyimides.[54]

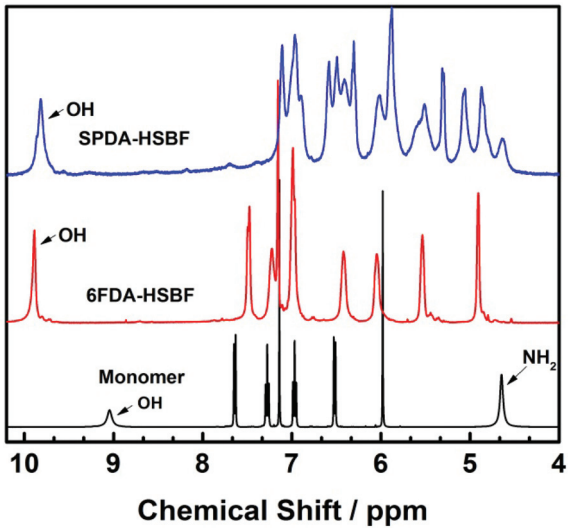

Fig. 1 ^{1}H NMR of the HSBF monomer and HSBF-based polyimides, DMSO-d_6 was used as the solvent.

HSBF-based polyimides exhibit very good solubility in a variety of conventional solvents such as NMP, *m*-cresol, DMF, DMSO and THF, *etc.* They can readily be cast into transparent membranes. Similar to most aromatic polyimides, HSBF-based polymers exhibit good thermal stability with no weight loss below 380 °C (Fig. 2).

As previously reported, *o*-hydroxyl containing polyimides can be converted to polybenzoxazoles by thermal rearrangement.[42] The online mass spectroscopy following the TGA during heating of HSBF-based polyimides is shown in Fig. 3. It is interesting to note that the two polymers exhibited quite different thermal rearrangement behavior. When 6FDA was selected as dianhydride, the evolution of CO_2 (corresponding to the TR-induced PBO formation) started at 380 °C and reached a maximum at 420 °C (Fig. 3a). The isothermal TGA of 6FDA-HSBF at 420 °C (Fig. 3c) indicates that the TR process

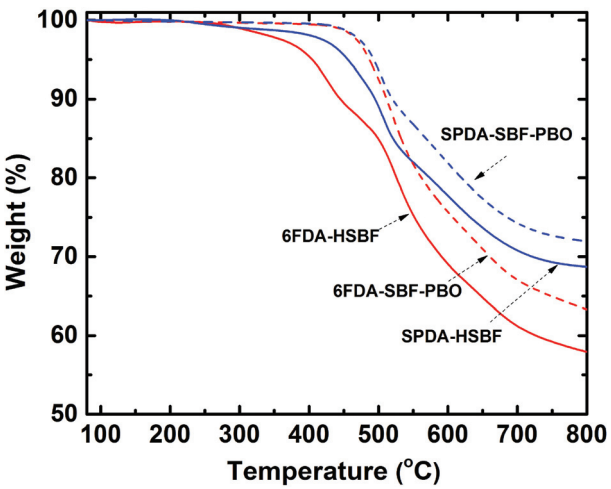

Fig. 2 TGA curve of the pristine and thermally rearranged polymer membranes.

was complete after 4 hours as identified by reaching the theoretical weight loss value of 11.2% due to CO_2 loss (100% formation of PBO). On the other hand, when the more bulky SPDA was chosen as dianhydride, the evolution of CO_2 started around 400 °C, about 20 °C higher than 6FDA-HSBF. Furthermore, there is evidence of bimodality during the CO_2 evolving process, accompanied with H_2O loss immediately generated around 460 °C (Fig. 3b), corresponding to the decomposition of the polymer main chain.[51] The isothermal TGA of SPDA-HSBF at 450 °C (Fig. 3d) indicates that after 2 hours, the TR was complete by reaching the theoretical weight loss of 9%.

The PBO formation of the polymers by the TR process was further confirmed by FT-IR, as shown in Fig. S1.† The hydroxyl stretching bond (between 3200 to 3600 cm^{-1}) and imide group (around 1780 cm^{-1}) disappeared during PBO formation, while the other two characteristic peaks of PBO (1555 cm^{-1} and 1064 cm^{-1}) emerged.[42] Similar to all previously reported TR polymers, they exhibited very good chemical stability, *e.g.*, they were insoluble in any conventional solvent (Table S1†). In addition, the PBOs also exhibited better thermal stability (Fig. 2) than their polyimide precursors with no thermal decomposition observed below 450 °C (Table 1).

The porosity of the polymers before and after PBO formation was evaluated by nitrogen adsorption/desorption, as shown in Fig. 4. The 6FDA-based polyimide (6FDA-HSBF) exhibits a relatively low BET surface area of 70 m^2 g^{-1}, whereas the SPDA-based polyimide (SPDA-HSBF) has a surface area of 464 m^2 g^{-1}, which is among the highest for hydroxyl-containing polyimides to date. After PBO formation, there is an expected increase of the surface area for the two polymers. In the case of the low surface area 6FDA-HSBF precursor, the corresponding 6FDA-SBF-PBO exhibited a 6-fold enhancement in surface area (from 70 to 417 m^2 g^{-1}). On the other hand, the relatively high surface area precursor SPDA-HSBF yielded only a small increase in BET surface area of less than 5% for SPDA-SBF-PBO (from 464 to 480 m^2 g^{-1}). A previously reported microporous spirobisindane-based polyimide, PIM-6FDA-OH, also showed a relatively small increase in surface area for the PBO counterpart (6FDA-SP-PBO) from 368 to 466 m^2 g^{-1} (Scheme 1).[51]

The significantly different structural changes induced by the TR process were also identified by wide-angle X-ray scattering results, as shown in Fig. S2.† The X-ray peaks give some information about the prevalent chain center-to-center distance. Similar to previously reported TR results, the main halo peak of 6FDA-HSBF (*d*-spacing = 5.59 Å) moved to a lower angle for the 6FDA-SBF-PBO (*d*-spacing = 5.75 Å); moreover, an additional halo emerged at an even smaller angle corresponding to the *d*-spacing of 7.8 Å. However, in the case of SPDA-HSBF and SPDA-SBF-PBO, the X-ray scattering signals were almost identical before and after TR, which agrees qualitatively well with the trends in the BET surface area results discussed above.

Gas permeation properties

To evaluate the effect of hydroxyl functionalization on the gas transport properties of the polyimide precursors, as well as

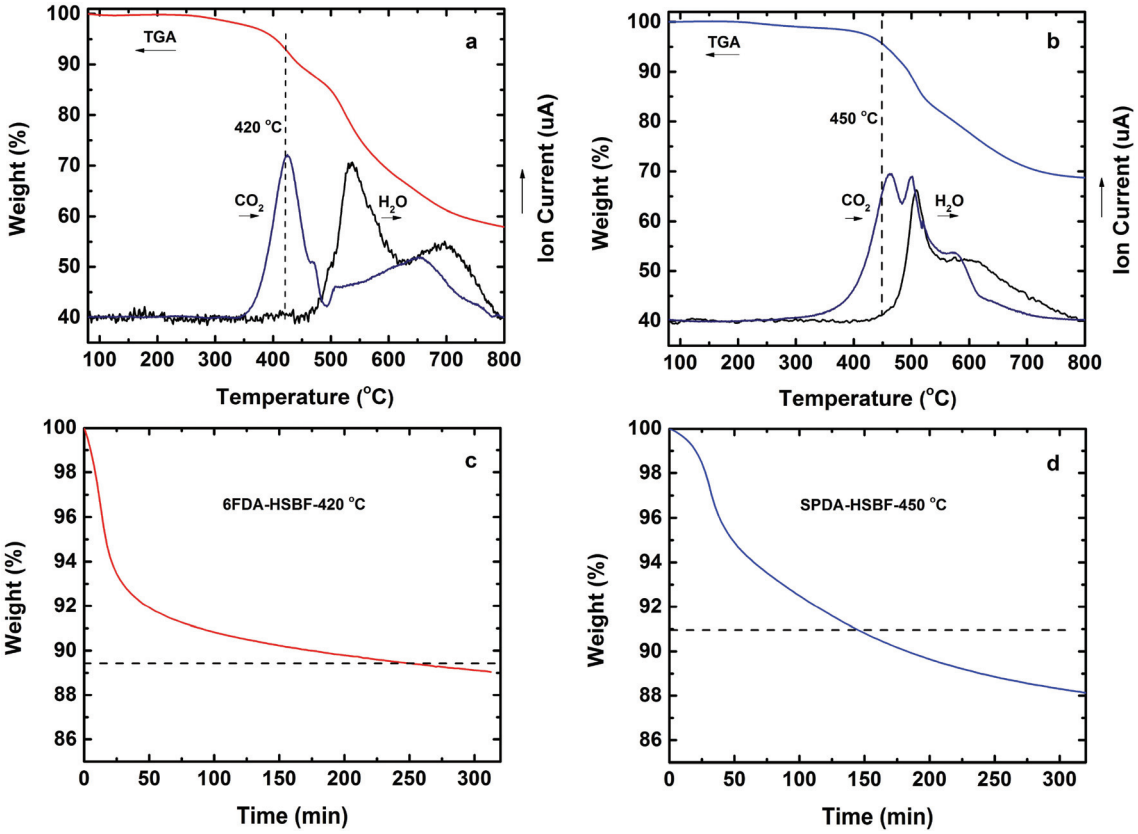

Fig. 3 TGA-QMS and isothermal TGA analysis of the 6FDA-HSBF and SPDA-HSBF polyimides. (a) TGA-QMS analysis of 6FDA-HSBF under N_2 atmosphere at a heating rate of 3 °C min^{-1}; (b) TGA-QMS analysis of SPDA-HSBF under a N_2 atmosphere at a heating rate of 3 °C min^{-1}; (c) isothermal TGA analysis of 6FDA-HSBF at 420 °C for 5 h under a N_2 atmosphere (the dashed line is the theoretical weight loss for complete PBO conversion). (d) Isothermal TGA analysis of 6FDA-HSBF at 450 °C for 5 h under a N_2 atmosphere (the dashed line is the theoretical weight loss for complete PBO conversion).

Table 1 Basic properties of the HSBF-based polyimides and their corresponding PBOs

Polymers	$M_n \times 10^{-4}$ (g mol^{-1})	PDI	T_d (°C)	S_{BET} (m^2 g^{-1})
6FDA-HSBF	2.89	2.41	380	70
SPDA-HSBF	4.24	2.30	400	464
6FDA-SBF-PBO	—	—	450	417
SPDA-SBF-PBO	—	—	450	480

their effect on the performance of the resulting PBOs, pure-gas permeabilities of H_2, N_2, O_2, CH_4 and CO_2 were obtained by the constant-volume/variable-pressure method and the results are shown in Table 2. The permeability and selectivity of the non-hydroxyl-based polymers, that is, 6FDA-SBF and SPDA-SBF, have previously been reported.[52] Introduction of a spirobifluorene "kink" gives rise to improved permeability compared with conventional hydroxyl-containing polyimides. For example, 6FDA-HAB, 6FDA-BisAPAF and HPEI, exhibited CO_2 permeabilities of only 2.9, 17 and 8.6 Barrer,[45,55,56] respectively, whereas the polyimides based on HSBF had significantly higher CO_2 permeabilities (6FDA-HSBF = 100 Barrer; SPDA-HSBF = 568 Barrer). It is noteworthy that the CO_2 permeability of SFDA-HSBF is among the highest of all previously reported OH-containing polyimides. The introduction of OH groups in the polyimides resulted in significantly increased selectivity, that is, the CO_2/CH_4 selectivity of 6FDA-SBF increased by 80% from 27.3 to 41.2 for 6FDA-HSBF. In the case of SPDA-SBF and SPDA-HSBF, the CO_2/CH_4 selectivity increased from 14.9 to 19.6 (Table 2).

It is interesting to note that hydroxyl- or PBO modification of the polyimides resulted in only minor differences in CO_2/N_2 selectivity (ranging from 21 to 26). The effect of the hydroxyl group on the gas permeability was strongly dependent on the BET surface area of the polymers. The low BET surface area 6FDA-HSBF membrane showed a 45% decrease in CO_2 permeability from 182 Barrer (6FDA-SBF) to 100 Barrer. On the other hand, the effect of the OH group on the permeability of the relatively high BET surface area SPDA-HSBF was much less pronounced, *e.g.*, P_{CO_2} for SPDA-SBF and SPDA-HSBF were 614 and 568, respectively, a drop of only 8%.

When the HSBF-based polyimide membranes were heat-treated to form PBOs, the permeabilities increased whereas the selectivities decreased, as expected based on previous reports. For 6FDA-SBF-PBO, a 12-fold increase in CO_2 permeability was observed relative to that of the 6FDA-HSBF precursor. This relative increase in CO_2 permeability is lower

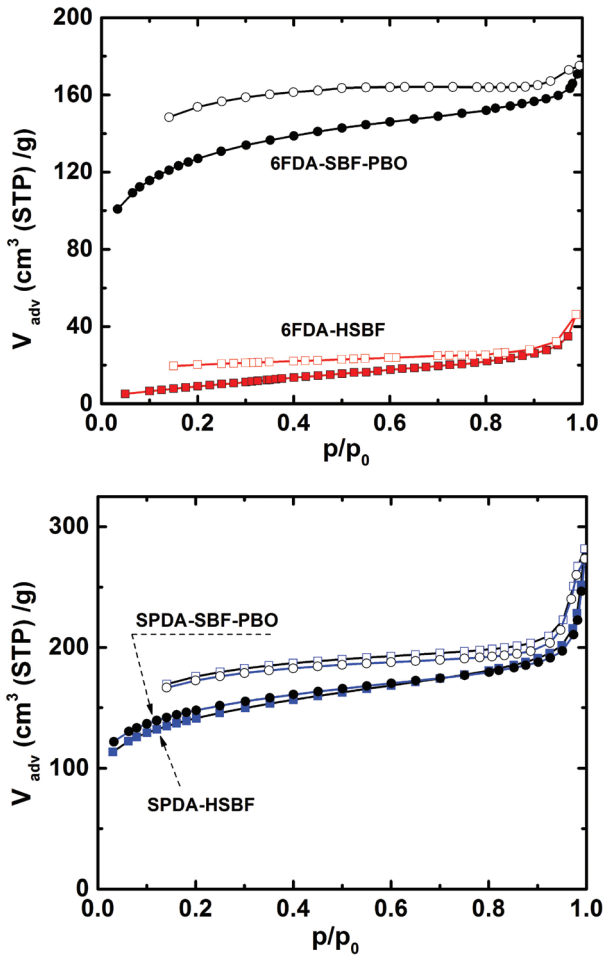

Fig. 4 N_2 adsorption/desorption isotherms of HSBF-based polyimides and PBOs.

than that of low permeability polymers, such as 6FDA-BisAPAF or 6FDA-HAB, which showed ~30- to 100-fold improvement in CO_2 permeability after PBO formation.[42,57] The CO_2/CH_4 selectivity of 6FDA-SBF-PBO dropped to about 50% of that of 6FDA-HSBF. This significant decrease in selectivity had previously been reported for 6FDA-bisAPAF- and 6FDA-HAB-based PBO membranes.[44,57] The relatively high BET surface area *o*-OH-functionalized polyimide precursor (SFDA-HSBF) showed a much smaller relative increase in permeability of the resulting PBO; *e.g.* the CO_2 permeability of SPDA-SBF-PBO increased only about 2-fold, from 568 to 1279 Barrer coupled with a drop in CO_2/CH_4 selectivity from 19.6 to 15.1. The overall performance of the *o*-OH-functionalized polyimide precursors and thermally-treated PBO membranes for CO_2/CH_4 separation is shown in Fig. 5. The HBSF-based polyimide precursor membranes and their counterpart PBO analogues show good CO_2/CH_4 separation properties, close to the 2008 Robeson upper bound.

The selectivity determined from pure-gas permeation measurements ($\alpha_{X/Y}$) involves contributions from the solubility selectivity (S_X/S_Y) and diffusion selectivity (D_X/D_Y). To better understand the role of hydroxyl groups in increasing CO_2/CH_4 selectivity, diffusion coefficients (D) and solubility coefficients (S) of SBF-PIs, HSBF-PIs and HSBF-based PBO membranes are summarized in Table 3. Although the *o*-OH-containing HSBF-based polyimides have a smaller BET surface area, they exhibit about the same solubility (S) for CO_2 and CH_4 compared to the non-hydroxyl SBF-based polymers. The lower permeability of *o*-OH-functionalized polyimides was mainly caused by a decrease in the diffusion coefficients (D); however, concurrently, it results in a tighter, more size-sieving structure, which leads to an increase in the diffusion selectivity α_D.

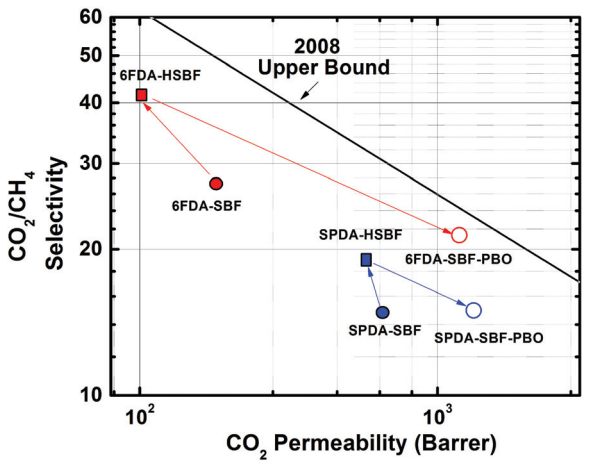

Fig. 5 CO_2/CH_4 separation performances of SBF- and HSBF-based polyimides and corresponding PBOs.

Table 2 Permeability and selectivity of SBF- and HSBF-based polyimide and PBO membranes for different gases at 35 °C

	Permeability (Barrer)[a]					Selectivity (α)			
Polymers	H_2	N_2	O_2	CH_4	CO_2	H_2/N_2	O_2/N_2	CH_4/N_2	CO_2/N_2	CO_2/CH_4
6FDA-SBF[b]	234	7.8	35.1	6.4	182	30.0	4.5	0.8	23.3	27.3
6FDA-HSBF	162	3.8	19.3	2.4	100	42.5	5.1	0.6	26.3	41.7
6FDA-SBF-PBO[c]	985	55	215	56	1160	17.9	3.9	1.0	21.1	20.7
SPDA-SBF[b]	501	28.6	111	41.1	614	17.5	3.9	1.4	21.5	14.9
SPDA-HSBF	519	24	98	29	568	21.6	4.1	1.2	23.7	19.6
SPDA-SBF-PBO[d]	775	61.6	225	84.8	1280	12.5	3.7	1.4	20.8	15.1
6FDA-SP-PBO[e]	429	30	120	34	675	14.3	4.2	1.1	22.0	20

[a] 1 Barrer = 10^{-10} cm^3(STP) cm cm^{-2} s^{-1} cm Hg^{-1} or 7.5×10^{-18} m^3(STP) m m^{-2} s^{-1} Pa^{-1}. [b] Ref. 52. [c] PBO formation was carried out at 420 °C for 4 h. [d] PBO formation was carried out at 450 °C for 2 h. [e] Ref. 51.

Table 3 Diffusion coefficient (D), solubility coefficient (S), diffusion selectivity (α_D) and solubility selectivity (α_S) for SBF- and HSBF-based polyimide and PBO membranes

	D^a (10^{-8} cm^2 s^{-1})			S^b (10^{-2} cm^3 cm^{-3} cmHg^{-1})			α_D	α_S
Polymers	N_2	CH_4	CO_2	N_2	CH_4	CO_2	CO_2/CH_4	CO_2/CH_4
6FDA-SBF	5.2	1.2	7.2	1.5	5.3	25	6.0	4.7
6FDA-HSBF	2.57	0.46	3.71	1.48	5.17	26.8	8.1	5.2
6FDA-SBF-PBO	14.7	3.91	22.6	3.75	14.4	51.1	5.8	3.6
SPDA-SBF	15	4.76	19.6	1.9	8.64	31.2	4.1	3.6
SPDA-HSBF	11.0	3.19	17.5	2.16	9.27	32.4	5.5	3.5
SPDA-SBF-PBO	16.2	5.16	21.7	3.79	16.4	58.9	4.2	3.6

[a] D was determined by the time-lag method. [b] S was deduced from the equation $P = D \times S$.

When the *o*-OH polyimides were converted to PBO membranes, the low surface area 6FDA-HSBF membrane exhibited a significant increase in the diffusion coefficients (*e.g.* D_{CO_2} increased 6-fold, from 3.71×10^{-8} cm^2 s^{-1} to 22.6×10^{-8} cm^2 s^{-1}) as well as solubility coefficient from 26.8×10^{-2} to 51.1×10^{-2} cm^3 cm^{-3} cmHg^{-1}. However, for the high BET surface area SPDA-HSBF membrane, only a small increase in the diffusion coefficient of CO_2 (from 17.5×10^{-8} cm^2 s^{-1} to 21.7×10^{-8} cm^2 s^{-1}) and solubility coefficient (from 32.4×10^{-2} to 58.9×10^{-2} cm^3 cm^{-3} cmHg^{-1}) was observed.

Conclusions

A spirobifluorene-based *o*-dihydroxyl-functionalized diamine (HSBF) was synthesized and two novel hydroxyl-containing polyimides were obtained by reaction with two dianhyrides (6FDA and SPDA). Both polyimides (6FDA-HSBF and SPDA-HSBF) exhibited good solubility in organic solvents and had high thermal stability. The BET surface area of the polyimides depended strongly on the choice of the dianhydride (6FDA-HSBF = 70 m^2 g^{-1} and SPDA-HSBF = 464 m^2 g^{-1}). Hydroxyl-functionalization (HSBF) resulted in polyimides with higher selectivity compared to their non-functionalized analogues (SBF) due to an increase in their diffusivity selectivity. PBOs formed by thermal treatment of HSBF-based polyimides showed higher gas permeability but at the expense of significantly reduced selectivity. This study suggests that the higher the microporosity of the pristine hydroxyl-containing polyimide, the smaller is the effect on the structural changes occurring during PBO formation by thermal rearrangement.

Acknowledgements

The authors acknowledge KAUST funding for Professor Ingo Pinnau.

Notes and references

1 P. Bernardo, E. Drioli and G. Golemme, *Ind. Eng. Chem. Res.*, 2009, **48**, 4638–4663.
2 R. W. Baker and K. Lokhandwala, *Ind. Eng. Chem. Res.*, 2008, **47**, 2109–2121.
3 R. W. Baker, *Ind. Eng. Chem. Res.*, 2002, **41**, 1393–1411.
4 L. M. Robeson, *J. Membr. Sci.*, 2008, **320**, 390–400.
5 L. M. Robeson, *J. Membr. Sci.*, 1991, **62**, 165–185.
6 T. Masuda, E. Isobe, T. Higashimura and K. Takada, *J. Am. Chem. Soc.*, 1983, **105**, 7473–7474.
7 I. Pinnau and L. G. Toy, *J. Membr. Sci.*, 1996, **116**, 199–209.
8 I. Pinnau, C. G. Casillas, A. Morisato and B. D. Freeman, *J. Polym. Sci., Part B: Polym. Phys.*, 1997, **35**, 1483–1490.
9 K. Nagai, T. Masuda, T. Nakagawa, B. D. Freeman and I. Pinnau, *Prog. Polym. Sci.*, 2001, **26**, 721–798.
10 P. M. Budd, E. S. Elabas, B. S. Ghanem, S. Makhseed, N. B. McKeown, K. J. Msayib, C. E. Tattershall and D. Wang, *Adv. Mater.*, 2004, **16**, 456–460.
11 P. M. Budd, B. S. Ghanem, S. Makhseed, N. B. McKeown, K. J. Msayib and C. E. Tattershall, *Chem. Commun.*, 2004, 230–231.
12 N. B. McKeown and P. M. Budd, *Chem. Soc. Rev.*, 2006, **35**, 675–683.
13 P. Budd, K. Msayib, C. Tattershall, B. Ghanem, K. Reynolds, N. McKeown and D. Fritsch, *J. Membr. Sci.*, 2005, **251**, 263–269.
14 P. Budd, N. McKeown, B. Ghanem, K. Msayib, D. Fritsch, L. Starannikova, N. Belov, O. Sanfirova, Y. Yampolskii and V. Shantarovich, *J. Membr. Sci.*, 2008, **325**, 851–860.
15 S. Thomas, I. Pinnau, N. Du and M. D. Guiver, *J. Membr. Sci.*, 2009, **333**, 125–131.
16 S. Thomas, I. Pinnau, N. Y. Du and M. D. Guiver, *J. Membr. Sci.*, 2009, **338**, 1–4.
17 N. Du, G. P. Robertson, J. Song, I. Pinnau, S. Thomas and M. D. Guiver, *Macromolecules*, 2008, **41**, 9656–9662.
18 N. Du, J. Song, G. P. Robertson, I. Pinnau and M. D. Guiver, *Macromol. Rapid Commun.*, 2008, **29**, 783–788.
19 N. Du, G. P. Robertson, I. Pinnau and M. D. Guiver, *Macromolecules*, 2009, **42**, 6023–6030.
20 N. Du, G. P. Robertson, J. Song, I. Pinnau and M. D. Guiver, *Macromolecules*, 2009, **42**, 6038–6043.
21 N. Du, G. P. Robertson, I. Pinnau and M. D. Guiver, *Macromolecules*, 2010, **43**, 8580–8587.
22 N. Du, H. B. Park, G. P. Robertson, M. M. Dal-Cin, T. Visser, L. Scoles and M. D. Guiver, *Nat. Mater.*, 2011, **10**, 372–375.

23 N. Du, H. B. Park, M. M. Dal-Cin and M. D. Guiver, *Energy Environ. Sci.*, 2012, **5**, 7306–7322.
24 C. R. Mason, L. Maynard-Atem, N. M. Al-Harbi, P. M. Budd, P. Bernardo, F. Bazzarelli, G. Clarizia and J. C. Jansen, *Macromolecules*, 2011, **44**, 6471–6479.
25 C. R. Mason, L. Maynard-Atem, K. W. Heard, B. Satilmis, P. M. Budd, K. Friess, M. Lanc, P. Bernardo, G. Clarizia and J. C. Jansen, *Macromolecules*, 2014, **47**, 1021–1029.
26 B. S. Ghanem, N. B. McKeown, P. M. Budd and D. Fritsch, *Macromolecules*, 2008, **41**, 1640–1646.
27 M. Carta, K. J. Msayib, P. M. Budd and N. B. McKeown, *Org. Lett.*, 2008, **10**, 2641–2643.
28 M. Carta, K. J. Msayib and N. B. McKeown, *Tetrahedron Lett.*, 2009, **50**, 5954–5957.
29 R. Short, M. Carta, C. G. Bezzu, D. Fritsch, B. M. Kariuki and N. B. McKeown, *Chem. Commun.*, 2011, **47**, 6822–6824.
30 C. G. Bezzu, M. Carta, A. Tonkins, J. C. Jansen, P. Bernardo, F. Bazzarelli and N. B. McKeown, *Adv. Mater.*, 2012, **24**, 5930–5934.
31 M. Carta, R. Malpass-Evans, M. Croad, Y. Rogan, J. C. Jansen, P. Bernardo, F. Bazzarelli and N. B. McKeown, *Science*, 2013, **339**, 303–307.
32 B. S. Ghanem, R. Swaidan, X. Ma, E. Litwiller and I. Pinnau, *Adv. Mater.*, 2014, DOI: 10.1002/adma.201401328.
33 M. Carta, M. Croad, R. Malpass-Evans, J. C. Jansen, P. Bernardo, G. Clarizia, K. Friess, M. Lanc and N. B. McKeown, *Adv. Mater.*, 2014, **26**, 3526–3531.
34 B. S. Ghanem, N. B. McKeown, P. M. Budd, J. D. Selbie and D. Fritsch, *Adv. Mater.*, 2008, **20**, 2766–2770.
35 B. S. Ghanem, N. B. McKeown, P. M. Budd, N. M. Al-Harbi, D. Fritsch, K. Heinrich, L. Starannikova, A. Tokarev and Y. Yampolskii, *Macromolecules*, 2009, **42**, 7881–7888.
36 Y. Rogan, L. Starannikova, V. Ryzhikh, Y. Yampolskii, P. Bernardo, F. Bazzarelli, J. C. Jansen and N. B. McKeown, *Polym. Chem.*, 2013, **4**, 3813.
37 Y. J. Cho and H. B. Park, *Macromol. Rapid Commun.*, 2011, **32**, 579–586.
38 S. A. Sydlik, Z. H. Chen and T. M. Swager, *Macromolecules*, 2011, **44**, 976–980.
39 B. S. Ghanem, R. Swaidan, E. Litwiller and I. Pinnau, *Adv. Mater.*, 2014, **22**, 3688–3692.
40 R. Swaidan, M. Al-Saeedi, B. Ghanem, E. Litwiller and I. Pinnau, *Macromolecules*, 2014, **47**, 5104–5114.
41 Y. Rogan, R. Malpass-Evans, M. Carta, M. Lee, J. C. Jansen, P. Bernardo, G. Clarizia, E. Tocci, K. Friess, M. Lanc and N. B. McKeown, *J. Mater. Chem. A*, 2014, **2**, 4874–4877.
42 H. B. Park, C. H. Jung, Y. M. Lee, A. J. Hill, S. J. Pas, S. T. Mudie, E. Van Wagner, B. D. Freeman and D. J. Cookson, *Science*, 2007, **318**, 254–258.
43 H. B. Park, S. H. Han, C. H. Jung, Y. M. Lee and A. J. Hill, *J. Membr. Sci.*, 2010, **359**, 11–24.
44 R. Guo, D. F. Sanders, Z. P. Smith, B. D. Freeman, D. R. Paul and J. E. McGrath, *J. Mater. Chem. A*, 2013, **1**, 262–272.
45 M. Calle and Y. M. Lee, *Macromolecules*, 2011, **44**, 1156–1165.
46 S. H. Han, J. E. Lee, K. J. Lee, H. B. Park and Y. M. Lee, *J. Membr. Sci.*, 2010, **357**, 143–151.
47 Z. P. Smith, D. F. Sanders, C. P. Ribeiro, R. Guo, B. D. Freeman, D. R. Paul, J. E. McGrath and S. Swinnea, *J. Membr. Sci.*, 2012, **415–416**, 558–567.
48 T. M. Moy and J. E. Mcgrath, *J. Polym. Sci., Part A: Polym. Chem.*, 1994, **32**, 1903–1908.
49 H. Shamsipur, B. A. Dawood, P. M. Budd, P. Bernardo, G. Clarizia and J. C. Jansen, *Macromolecules*, 2014, **47**, 5595–5606.
50 X. Ma, R. Swaidan, Y. Belmabkhout, Y. Zhu, E. Litwiller, M. Jouiad, I. Pinnau and Y. Han, *Macromolecules*, 2012, **45**, 3841–3849.
51 S. Li, H. J. Jo, S. H. Han, C. H. Park, S. Kim, P. M. Budd and Y. M. Lee, *J. Membr. Sci.*, 2013, **434**, 137–147.
52 X. Ma, O. Salinas, E. Litwiller and I. Pinnau, *Macromolecules*, 2013, **46**, 9618–9624.
53 F. Thiemann, T. Piehler, D. Haase, W. Saak and A. Lutzen, *Eur. J. Org. Chem.*, 2005, 1991–2001.
54 M. Calle and Y. M. Lee, *Macromolecules*, 2011, **44**, 1156–1165.
55 R. Guo, D. F. Sanders, Z. P. Smith, B. D. Freeman, D. R. Paul and J. E. McGrath, *J. Mater. Chem. A*, 2013, **1**, 6063–6072.
56 C. H. Jung and Y. M. Lee, *Macromol. Res.*, 2008, **16**, 555–560.
57 S. H. Han, N. Misdan, S. Kim, C. M. Doherty, A. J. Hill and Y. M. Lee, *Macromolecules*, 2010, **43**, 7657–7667.

